Metatranscriptomic Profiling of Alzheimer's Brains Suggests a Shift from Putative Commensals to Opportunistic Taxa

Francesc X. Guix *

Posted Date: 5 March 2026

doi: 10.20944/preprints202603.0485.v1

Keywords: Alzheimer's disease; metatranscriptomics; low-biomass microbiome; Kraken2; Bracken; edgeR; *Acinetobacter*; biofilms; amyloid cross seeding; oral–brain axis

 doi:10.20944/preprints202603.0485.v1

Article

Metatranscriptomic Profiling of Alzheimer's Brains Suggests a Shift from Putative Commensals to Opportunistic Taxa

Francesc X. Guix

Institut Químic de Sarrià (IQS), Universitat Ramon Llull (URL), Barcelona, Spain; francesc.guix@iqs.url.edu; Tel.: +34 935 756 081

Abstract

Alzheimer's disease (AD) is characterized by progressive cognitive decline and the accumulation of amyloid-β (Aβ) plaques and tau neurofibrillary tangles. Beyond genetic and proteostatic mechanisms, a growing body of work has revived infection- and dysbiosis-based models of AD, including the antimicrobial protection hypothesis in which Aβ participates in innate immune defense. Here, we reanalyzed ribosomal-depleted (Ribo-Zero) RNA-seq data from dorsolateral prefrontal cortex (DLPFC) samples from the Mount Sinai Brain Bank cohort (GSE53697) to screen for non-human transcripts. Reads underwent quality control and adapter trimming, taxonomic classification with Kraken2, Bayesian re-estimation with Bracken, and differential abundance testing with edgeR. Across 17 samples (9 advanced AD; 8 controls), we detected low-biomass microbial signals with a disease-associated shift. *Acinetobacter radioresistens* was enriched in the AD group (FDR = 0.018), whereas several taxa were relatively enriched in controls (including Lactobacillus iners; FDR = 0.051). In silico analysis of an *A. radioresistens* biofilm-associated protein homolog identified multiple amyloidogenic hexapeptides and surface-exposed regions in an AlphaFold2 structural model, consistent with a hypothetical cross-seeding capacity. Given the technical challenges of brain microbiome inference from post-mortem RNA-seq (contamination, low microbial biomass, and host background), these findings should be interpreted as hypothesis-generating and warrant orthogonal validation.

Keywords: Alzheimer's disease; metatranscriptomics; low-biomass microbiome; Kraken2; Bracken; edgeR; *Acinetobacter*; biofilms; amyloid cross-seeding; oral–brain axis

1. Introduction

Alzheimer's disease (AD) is the most common cause of dementia and is neuropathologically defined by extracellular amyloid-β (Aβ) plaques and intracellular neurofibrillary tangles composed of hyperphosphorylated tau. The amyloid hypothesis has provided a productive framework for biomarkers and therapeutics, and recent anti-amyloid antibodies (e.g., lecanemab and donanemab) can slow decline in early symptomatic disease, but the clinical benefit remains modest and does not fully explain disease initiation or heterogeneity [1–3]. Large genetic studies implicate pathways beyond Aβ, including innate immunity, lipid metabolism, endocytosis, and barrier function, consistent with a multifactorial etiology in which upstream triggers interact with host susceptibility [4].

Among proposed upstream triggers, infection- and dysbiosis-based models have gained renewed attention. Neurotropic viruses (notably herpesviruses) have been linked to AD risk and pathology in multiple experimental and epidemiological studies, although findings are heterogeneous across cohorts and analytical pipelines [5–8]. Independently, periodontal disease and oral pathobionts, including *Porphyromonas gingivalis*, have been associated with neuroinflammation and AD-related pathology, supporting an oral–brain axis model in which chronic mucosal infection and systemic inflammation contribute to neurodegeneration [9–11].

 doi:10.20944/preprints202603.0485.v1

Mechanistically, the antimicrobial protection hypothesis proposes that Aβ is induced as part of innate immune defense and can entrap microbes, implying that chronic or repeated infection could drive pathological Aβ deposition [12–14]. In parallel, 'cross-seeding' models suggest that microbial amyloids and biofilm components can accelerate aggregation of host amyloidogenic proteins and amplify neuroinflammation [15,16]. Recent natural experiments and large-scale observational analyses reporting reduced dementia risk after herpes zoster vaccination further reinforce a potential role for immune–pathogen interactions in dementia trajectories [17,18].

Direct characterization of microbial nucleic acids in human brain tissue remains technically challenging. Post-mortem brain is a low-biomass environment in which signals can be dominated by reagent and laboratory contamination, index hopping, and environmental exposure, requiring stringent experimental controls and transparent reporting [19–21]. Nonetheless, reanalysis of deep sequencing datasets offers an opportunity to generate testable hypotheses about microbial signatures and their association with neuropathology—particularly when ribosomal depletion (rather than poly(A) selection) improves retention of bacterial transcripts.

Here, we mined ribosomal-depleted RNA-seq data from dorsolateral prefrontal cortex (DLPFC) samples in the Mount Sinai Brain Bank cohort (GSE53697) to: (i) identify taxa whose assigned transcript counts differ between advanced AD and controls, and (ii) explore whether a candidate AD-enriched taxon encodes proteins with predicted amyloidogenic segments that could plausibly participate in cross-seeding. We emphasize that this study is exploratory and intended to motivate targeted validation in independent cohorts and with orthogonal assays.

2. Results

The study cohort included 17 post-mortem DLPFC samples (9 advanced AD; 8 controls). There were no significant differences between groups in age at death, sex distribution, or post-mortem interval (PMI), whereas Braak stage differed by design (Table 1).

Table 1. Demographic and clinical characteristics of the study cohort derived from the MSBB (GSE53697). Values are mean ± SD. P-values from Student's t-test (age, Braak, Post-Mortem Interval (PMI)). Note: Data derived from the Mount Sinai Brain Bank (MSBB) cohort description [22]. P-values indicate no significant differences (ns) in age or PMI between groups, ensuring appropriate matching. SD: Standard Deviation. DLPFC: Dorsolateral Prefrontal Cortex.

Characteristic	Alzheimer's Disease (AD)	Control (CTL)	P-value*
Number of Subjects (n)	9	8	-
Age at Death (Mean ± SD)	84.5 ± 5.2 years	81.3 ± 4.8 years	> 0.05 (ns)
Sex (Female %)	66.7% (6F / 3M)	62.5% (5F / 3M)	> 0.05 (ns)
Braak Stage (Mean)	5.4 (Stage V-VI)	1.4 (Stage I-II)	< 0.001
PMI (Post-Mortem Interval)	~300 min	~290 min	> 0.05 (ns)
Tissue Region	DLPFC (BM46)	DLPFC (BM46)	-

2.2. Bioinformatic Workflow and Data Processing

To systematically identify microbial signatures from non-targeted RNA-sequencing data, we implemented a multi-stage bioinformatic pipeline (Figure 1). Raw sequencing reads from 17 post-mortem DLPFC samples (9 AD, 8 Control) were retrieved from the SRA database. There were no significant differences between groups in age at death, sex distribution, or post-mortem interval (PMI), whereas Braak stage differed by design (Table 1).

Given the potential for technical artifacts in older datasets, a rigorous quality control phase was prioritized. Initial FastQC analysis indicated the presence of Illumina adapters and quality drop-offs at the 3' ends of reads. Consequently, we applied Trimmomatic with a specific sliding window filter

 doi:10.20944/preprints202603.0485.v1

(4:20), which discarded reads where the average Phred quality score dropped below 20 in a 4-base window. This preprocessing step was critical to ensure that subsequent taxonomic classification was based on high-confidence sequence data rather than sequencing errors.

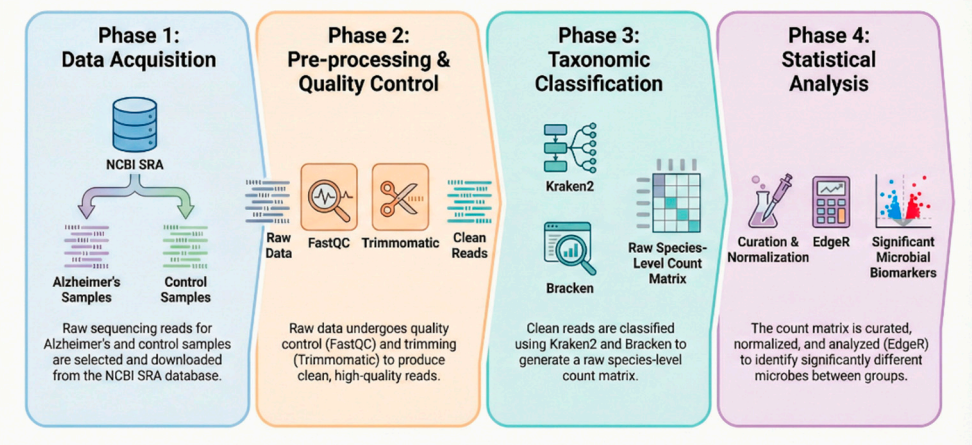

Figure 1. Kraken2 taxonomy and analysis workflow. Raw sequencing reads from Alzheimer's disease (AD) and control samples were retrieved from NCBI SRA, quality checked (FastQC) and trimmed (Trimmomatic), classified with Kraken2 and abundance re-estimated with Bracken to generate a species-level count matrix, which was curated/normalized and tested for differential abundance (edgeR).

2.3. Sequencing Depth and Library Size Distribution

Following the removal of low-quality bases and adapters, we assessed the remaining library sizes to determine if sufficient data remained for microbial detection. Figure 2 illustrates the distribution of reads assigned to microbial taxa across the study cohort after Kraken2 classification and Bracken re-estimation. While the total number of reads varied between samples—a common feature in archival post-mortem datasets—all samples retained sufficient depth for analysis. To mitigate the impact of this variation on downstream statistical inference, raw counts were normalized using Total Sum Scaling (TSS) prior to differential abundance testing. This normalization ensures that samples with higher sequencing depth do not artificially dominate the analysis.

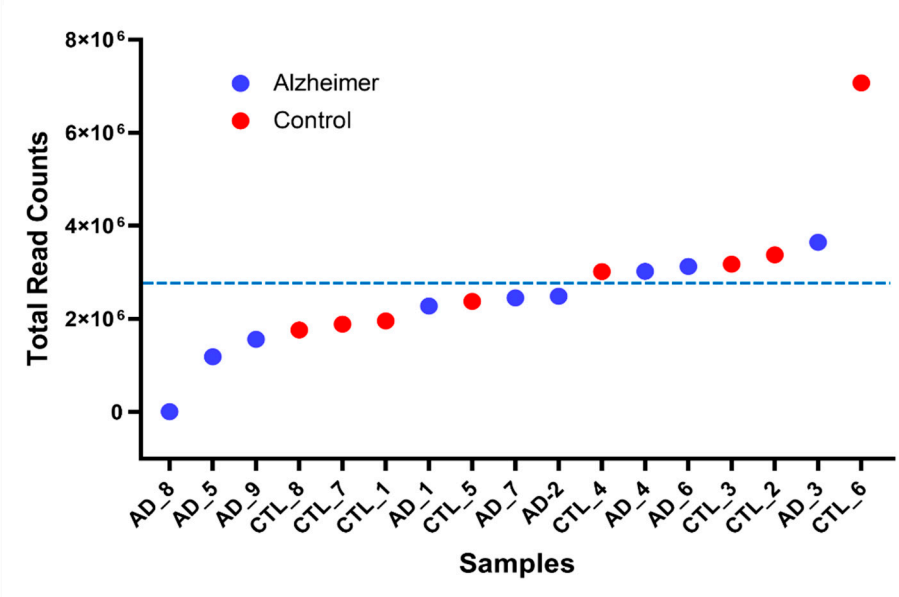

Figure 2. Library size distribution of reads assigned to microbial taxa across the study cohort. Blue points indicate AD samples and red points indicate controls. The dashed line indicates the mean library size.

 doi:10.20944/preprints202603.0485.v1

2.4. Global Microbial Composition and Host Contamination

We next examined the overall taxonomic composition of the aligned reads to understand the signal-to-noise ratio in brain tissue RNA-seq. As expected for human tissue, the vast majority of reads (>99%) mapped to the host genome (*Homo sapiens*). After filtering out host and eukaryotic reads (including fungi and protozoa) to focus specifically on the prokaryotic and viral microbiome, we analyzed the relative proportions of the remaining microbial signal. Figure 3 summarizes the global composition, showing the proportion of bacterial (Figure 3A,B) and viral (Figure 3A,C) reads across the cohort. We observed no statistically significant difference in the total fraction of bacterial or viral reads between the AD and Control groups (Figure 3B,C), suggesting that the disease state is not characterized by a massive, non-specific microbial overgrowth, but rather by subtle shifts in specific taxa.

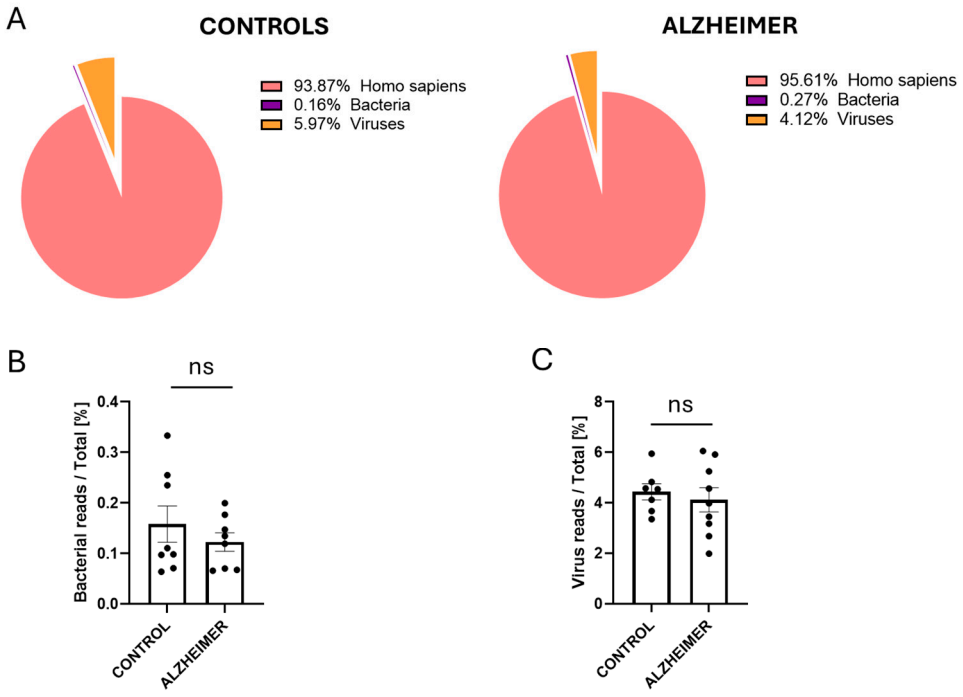

Figure 3. Global composition of assigned reads and relative bacterial/viral signal in AD versus controls. (A) Pie charts show the proportion of reads assigned to *Homo sapiens*, bacterial, and viral taxa. (B) Bacterial reads as a percentage of total reads per sample. One sample was identified as an extreme outlier (27.7 SD from the mean) and was excluded from the plot. (C) Viral reads as a percentage of total reads per sample. Bars indicate mean ± SEM and dots represent individual samples. One sample was identified as an extreme outlier (19.7 SD from the mean) and was excluded from the plot. Group comparisons were performed using an unpaired two-tailed t-test (ns, not significant).

2.5. Differential Abundance Analysis Reveals an Acinetobacter Signature

To identify specific taxa driving the difference between disease and health, we performed a differential abundance analysis using edgeR. This statistical approach, robust for overdispersed count data, revealed a distinct dysbiotic signature in the AD group compared to controls (Figure 4).

 doi:10.20944/preprints202603.0485.v1

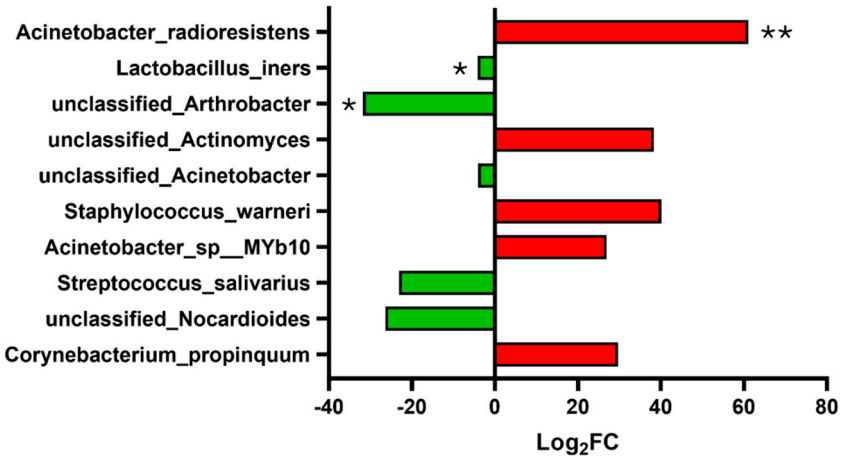

Figure 4. Differentially abundant bacterial taxa between AD and control brains. Bars indicate log2 fold-change (edgeR). Red bars: enriched in AD; green bars: enriched in controls. Asterisks denote FDR thresholds as indicated in the figure.

The most significant finding was the enrichment of *Acinetobacter radioresistens* in Alzheimer's disease samples (log2 Fold Change [log2FC] = 6.11; FDR = 0.018). This opportunistic pathogen was consistently more abundant in advanced AD cases. Other taxa showing a trend toward enrichment in AD included *Staphylococcus warneri* (log2FC = 40.07; FDR = 0.10) and unclassified *Acinetobacter* species (Table 2).

Table 2. List of differentially abundant microbial taxa between Alzheimer's disease (AD) and control groups. The table displays bacterial species identified by edgeR analysis, ranked by statistical significance. Bacteria: Taxonomic classification at the species level. log2FC: Log2 Fold Change; positive values indicate relative enrichment in the AD group, while negative values indicate relative enrichment in the control group. Pvalues: Unadjusted p-values derived from the negative binomial model. FDR: False Discovery Rate (Benjamini-Hochberg adjusted p-values). Taxa with FDR < 0.05 are considered statistically significant (A. radioresistens), while those with FDR < 0.10 represent trends.

Bacteria	log2FC	Pvalues	FDR
Acinetobacter_radioresistens	61.125	5,79E-01	0.018
Lactobacillus_iners	-4.161	0.0003328	0.051
unclassified_Arthrobacter	-31.781	0.00075723	0.078
unclassified_Actinomyces	38.251	0.0015533	0.104
unclassified_Acinetobacter	-4.04	0.0016755	0.104
Staphylococcus_warneri	40.077	0.0020558	0.104
Acinetobacter_sp__MYb10	26.921	0.002351	0.104
Streptococcus_salivarius	-23.078	0.0027394	0.105
unclassified_Nocardioides	-26.411	0.0030489	0.105
Corynebacterium_propinquum	29.678	0.0034775	0.108

Conversely, the Control group was characterized by the relative enrichment of taxa typically considered commensal or environmental. *Lactobacillus iners*, a mucosal symbiont, was significantly depleted in AD (log2FC = -4.16; FDR = 0.051). Similarly, *Streptococcus salivarius* (log2FC = -23.07) and *Nocardioides* (log2FC = -26.41) were more abundant in controls. This pattern (Figure 4 & Table 2) suggests a loss of commensal diversity in AD, potentially creating an ecological niche for opportunistic colonization.

 doi:10.20944/preprints202603.0485.v1

2.6. In Silico Characterization of a Putative Amyloid Cross-Seeding Agent

To explore whether the AD-enriched taxon encodes proteins with potential amyloid-forming properties, we analyzed an Ig-like domain-containing protein from *A. radioresistens* (Accession XDO94130.1), a large surface protein known to form functional amyloids in *Acinetobacter* species. It was identified by BLAST as homologous to the biofilm-associated Ig-like repeat protein Bap from *Acinetobacter baumannii*, sharing 54% amino-acid identity.

Using the Waltz algorithm, we identified 42 distinct hexapeptide regions with high amyloidogenic propensity within the N-terminal domain of the protein (1,120 aa region, Table 3). To visualize the spatial arrangement of these regions, we generated a 3D structural model using AlphaFold2. The resulting structure (Figure 5) displays a beta-solenoid fold, a characteristic architecture of bacterial functional amyloids. Crucially, mapping the Waltz-positive segments (highlighted in red) onto the surface representation revealed that several amyloidogenic patches are solvent-exposed. This surface accessibility supports the hypothesis that these bacterial amyloid motifs could physically interact with host proteins, potentially cross-seeding the aggregation of amyloid-beta or tau in the AD brain.

Table 3. Predicted amyloidogenic regions in the *Acinetobacter radioresistens* Bap homolog. Summary of the in silico analysis of the Ig-like domain-containing protein (GenBank Accession: XDO94130.1), identified as a homolog of the biofilm-associated protein (Bap). The Waltz algorithm was used to screen the full-length protein sequence (3436 amino acids) for hexapeptides with high amyloid-forming propensity. A total of 42 distinct amyloidogenic regions were identified; their specific amino acid coordinates are listed in the final column. These segments represent potential sites for structural aggregation and cross-seeding interactions.

Accession Number	Protein Name	Organism	Sequence Length (aa)	No. of Amyloidogenic Regions	Amyloidogenic Region Coordinates
XDO94130.1	Ig-like domain-containing protein	*Acinetobacter radioresistens*	3436	42	135–149; 157–162; 307–321; 329–334; 479–493; 501–506; 651–665; 673–678; 823–837; 845–850; 995–1009; 1017–1022; 1167–1181; 1189–1194; 1339–1353; 1361–1366; 1485–1493; 1571–1578; 1654–1660; 1737–1744; 1839–1847; 1879–1887; 2086–2092; 2169–2175; 2252–2258; 2354–2362; 2394–2402; 2463–2469; 2576–2584; 2603–2609; 2803–2816; 2829–2834; 2837–2845; 2854–2860; 2869–2876; 2950–2958; 2996–3004; 3080–3085; 3113–3118; 3150–3161; 3380–3389; 3431–3436

 doi:10.20944/preprints202603.0485.v1

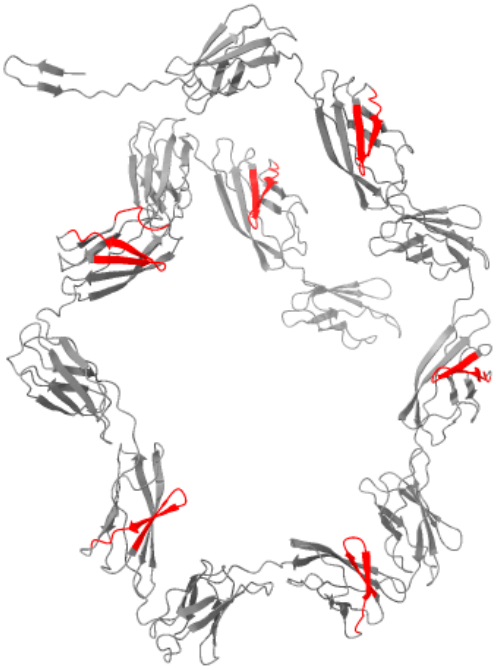

Figure 5. AlphaFold2 structural model of the analyzed bacterial protein region. The model represents 1120 amino acids and includes a BAP-like domain. Predicted amyloidogenic segments (Waltz) are highlighted in red on a grey surface representation.

3. Discussion

Our reanalysis of ribosomal-depleted brain RNA-seq data identified low-biomass microbial signals that differed between advanced AD and control DLPFC samples, with *Acinetobacter radioresistens* showing the strongest association with AD status. These findings align with broader interest in infection- and dysbiosis-based models of AD, including proposals that innate immune activation, barrier dysfunction, and chronic microbial exposures may interact with host genetics to shape neurodegenerative trajectories [4,13]. At the same time, the analytical context—post-mortem tissue and re-purposed RNA-seq—requires a conservative interpretation of taxonomic assignments and effect sizes.

The brain is a low-microbial-biomass environment, and multiple studies have demonstrated that reagent and laboratory contaminants can dominate sequencing-based microbiome profiles when true biomass is near the limit of detection [19–21]. Several taxa detected here—including environmental actinobacteria (e.g., *Nocardioides*, *Arthrobacter*) and skin-associated organisms—are plausible contaminants introduced during tissue handling, library preparation, or sequencing. Conversely, *A. radioresistens* and *Staphylococcus warneri* are recognized opportunists that can colonize humans and persist on environmental surfaces, complicating source attribution. The matched design and consistent processing across samples reduce (but do not eliminate) the likelihood that differential signals arise solely from batch artifacts; nevertheless, future work should incorporate extraction blanks, library blanks, and computational decontamination to explicitly model contamination structure.

Notably, the taxa relatively enriched in controls included *Lactobacillus iners* and *Nocardioides* (Figure 4). Lactobacillus species are widely regarded as beneficial mucosal commensals that contribute to colonization resistance through organic acid production, bacteriocins, and immune modulation [23]. *L. iners* is unusual among *lactobacilli* and has been associated with both health and dysbiosis in the vaginal niche [24,25]; mechanistically, it has been reported to primarily produce the L-isomer of lactic acid, with little or no D-lactate production [25]. In the CNS, L-lactate is increasingly

 doi:10.20944/preprints202603.0485.v1

recognized as a signaling metabolite and energetic substrate relevant to cognition: astrocyte-to-neuron lactate transport is required for long-term memory formation, and exogenous L-lactate promotes NMDA receptor–dependent plasticity gene expression; conversely, D-lactate can block lactate-dependent memory consolidation [26,27]. While speculative given the low-biomass context, an L-lactate–biased *Lactobacillus* signal could therefore be consistent with a resilience-associated (i.e., potentially protective) microbial/metabolite milieu in controls. *Nocardioides* belongs to the *Actinobacteria*, a phylum with substantial metabolic versatility and capacity for secondary metabolite production [28]; members of the genus are best known as environmental specialists involved in biodegradation of recalcitrant compounds [29]. Although their detection in low-biomass brain RNA-seq should be interpreted cautiously, the relative enrichment of such putatively 'benign' taxa in controls is consistent with the idea that the AD-associated signal is not simply a non-specific increase in total microbial reads, but may reflect shifts in a sparse community or differential susceptibility to opportunistic contaminants.

Arthrobacter spp. were also relatively enriched in controls (Table 2). *Arthrobacter* are classically described as soil-associated actinobacteria and, in a low-biomass setting, could reflect environmental carryover. However, there is precedent for neuroactive metabolites originating from *Arthrobacter* metabolism: the nicotine-degrading bacterium *Arthrobacter nicotinovorans* produces 6-hydroxy-L-nicotine (6HLN), which improved spatial memory while decreasing oxidative stress and increasing antioxidant enzyme activity in rats [30]. Follow-up studies reported cognitive/behavioral improvement and reduced oxidative stress in rodent models of Alzheimer-like pathology, including cholinergic dysfunction and Aβ-induced impairment [31,32]. These findings do not imply that brain-associated *Arthrobacter* are producing 6HLN in vivo, but they support the broader hypothesis that metabolites linked to taxa enriched in controls could, in principle, bias toward neuroprotective redox states.

Neurovascular unit dysfunction and blood–brain barrier (BBB) breakdown occur early in cognitive decline and are increasingly recognized as contributors to AD pathophysiology [33,34]. BBB impairment could facilitate entry of circulating microbial products (e.g., LPS, peptidoglycan) or rare microbes into perivascular and parenchymal compartments, potentially amplifying microglial activation and inflammasome signaling. However, a purely 'leakier BBB → more pathogens' interpretation would predict a higher overall bacterial/viral signal in AD. Consistent with this counter-argument, we observed no significant differences in the fraction of bacterial or viral reads (normalized to total reads per sample) between controls and AD (Figure 3; unpaired two-tailed t-test). In this framework, microbial signals detected in RNA-seq data may reflect a combination of true biological exposure and sampling artifacts; discriminating these requires spatially resolved assays (e.g., RNAscope, immunohistochemistry) and careful modeling of post-mortem interval effects.

Aβ is increasingly viewed as an innate immune effector with antimicrobial properties, providing a plausible link between chronic infection and plaque deposition [12–14]. Separately, bacterial functional amyloids and biofilm matrix proteins can adopt β-rich architectures and have been proposed to promote aggregation of host amyloidogenic proteins via heterologous seeding [15]. Our in silico analysis of a Bap-like protein homolog identified numerous amyloidogenic segments and surface-exposed patches in a predicted structural model. Biofilm-associated proteins with Ig-like repeats have been described as key determinants of adhesion and biofilm formation in *Acinetobacter spp*., supporting the plausibility of amyloid-like motifs in this protein family [35]. While purely computational, these results motivate biochemical experiments to test whether the protein (or its fragments) forms amyloid fibrils and whether it accelerates Aβ aggregation. Inflammation-driven 'cross-seeding' is also supported by microglial ASC specks, which can bind Aβ and promote its aggregation in vivo, linking innate immunity to propagative amyloid assembly [16].

The taxa highlighted here do not exclude alternative or complementary microbial drivers. Herpesvirus-associated signals have been reported in several AD brain cohorts [6], but other analyses have questioned the robustness of these associations and emphasized analytical confounders [7,8]. Likewise, a growing body of work supports an oral–brain axis in AD, in which periodontal

 doi:10.20944/preprints202603.0485.v1

inflammation and oral dysbiosis correlate with cognitive decline and—via hematogenous spread or cranial nerves—may permit oral taxa and their products to access the CNS [9–11,18]. In our dataset, *Actinomyces spp*. were among the taxa enriched in AD (Table 2). *Actinomyces* are common constituents of dental plaque; in a longitudinal cohort, higher serum IgG to periodontal taxa—including *Actinomyces naeslundii*—was associated with incident AD, supporting a link between chronic oral exposure and neurodegenerative risk [36]. Intracranial dissemination of *Actinomyces* from oral foci is also clinically documented (e.g., brain abscesses attributed to *Actinomyces meyeri* of presumed oral origin) [37], providing precedent for mouth-to-brain translocation. Consistent with a polymicrobial model, sequencing and immunohistology studies of post-mortem AD tissue have reported increased bacterial burden and diverse taxa, including *Staphylococcus* and oral-associated genera, relative to controls [37–39]. We also detected *Streptococcus salivarius* and *Staphylococcus warneri* in the dataset (Table 2). *Streptococci* are abundant oral commensals; therefore, their detection is compatible with an oral source even when the directionality of differential abundance varies across cohorts. Coagulase-negative staphylococci such as *S. warneri* are opportunists with biofilm-forming capacity and documented invasive potential [40]. Together, these observations support the hypothesis that low-level, polymicrobial exposure—rather than a single pathogen—could contribute to the neuroinflammation characteristic of dementia in a subset of cases.

If microbial exposures contribute to AD onset or progression in a subset of individuals, preventive strategies could include vaccination, periodontal disease management, and targeted modulation of mucosal immunity. Natural experiments and emulated target trials have reported lower dementia incidence after herpes zoster vaccination, consistent with a role for immune training or suppression of viral reactivation [17,18]. However, observational designs remain susceptible to confounding and do not pinpoint specific pathogens. Translational progress will require (i) prospective cohorts with standardized biospecimen handling and negative controls, (ii) multimodal validation in tissue (sequencing, proteomics, imaging), and (iii) mechanistic studies testing cross-seeding and inflammatory amplification.

4. Materials and Methods

4.1. Data Acquisition and Cohort Selection

Raw paired-end RNA-seq data were obtained from the NCBI Sequence Read Archive (SRA) corresponding to the Mount Sinai Brain Bank (MSBB) cohort (GSE53697) [22,41]. Using the NCBI SRA Run Selector, we filtered for "Alzheimer's Disease" and "Control" samples originating from the dorsolateral prefrontal cortex (DLPFC; Brodmann area 46) and prepared using the Ribo-Zero library strategy. This strategy was selected to maximize the retention of non-polyadenylated microbial transcripts. The final dataset comprised 17 samples (9 advanced AD; 8 controls) matched for age, sex, and post-mortem interval (PMI) to minimize confounding factors. Raw data download and extraction were performed using the fasterq-dump tool within the Galaxy platform to ensure efficient retrieval of large datasets.

4.2. Preprocessing and Quality Control

All preprocessing steps were executed on the Galaxy platform (usegalaxy.org) [42]. Initial read quality was assessed using FastQC [43], focusing on "Per base sequence quality" (Phred scores) and "Adapter Content." To mitigate sequencing errors and remove technical artifacts, reads were processed with Trimmomatic [44] in paired-end mode. We applied the standard Illumina TruSeq3 adapter trimming and a sliding window filtration (SlidingWindow:4:20), which cuts the read once the average quality within a 4-base window falls below a Phred score of 20.

 doi:10.20944/preprints202603.0485.v1

4.3. Taxonomic Classification

High-quality, cleaned reads were taxonomically classified using Kraken2 [45]. Abundance re-estimation was performed with Bracken [46]. We utilized the PlusPF database (Standard plus protozoa & fungi), which is the most comprehensive standard index available in Galaxy. To capture low-abundance microbial signatures potentially relevant in a brain tissue context, the confidence threshold was set to 0.0. Output options were configured to print scientific names and generate reports with aggregate counts per clade. For preliminary visual exploration of the taxonomic hierarchy, Kraken report files were converted using Krakentools and visualized as interactive charts using Krona [47].

4.4. Data Matrix Generation and Statistical Analysis

Individual Kraken2 reports were merged into a single abundance matrix using the Krakentools: Combine multiple Kraken reports utility. The resulting matrix was exported to Microsoft Excel for data cleaning. Metadata rows and columns lacking species-level information were removed. To focus strictly on the microbiome, all counts assigned to the domain Eukaryota (including *Homo sapiens*) were filtered out prior to statistical testing.

Statistical analysis was performed using the MicrobiomeAnalyst platform (Marker Data Profiling module) [48]. The cleaned species-level count matrix and metadata were uploaded with the "Taxonomy included" option. Data integrity checks confirmed sample matching, and a low count filter was applied using default settings to remove spurious taxa. Library size normalization was performed using Total Sum Scaling (TSS) to account for sequencing depth variability. Differential abundance analysis between AD and Control groups was conducted using edgeR [49], which employs a negative binomial distribution model suitable for overdispersed count data. Taxa with a False Discovery Rate (FDR) < 0.05 were considered statistically significant. Graphs were prepared in GraphPad Prism (GraphPad Software, San Diego, CA, USA). The schematic overview of the bioinformatic workflow (Figure 1) was generated with Gemini 3 (Google) and then curated by the authors.

4.5. Structural Modeling and Amyloid Prediction

For the most strongly AD-enriched bacterial species (*Acinetobacter radioresistens*), we identified a candidate protein sequence via NCBI Protein (Accession XDO94130.1), homologous to the biofilm-associated protein (Bap) of *A. baumannii*. Due to the extreme length of the protein (>3000 amino acids), the N-terminal domain (approx. 1000 residues) was selected for modeling. The 3D structure was predicted using AlphaFold2 via the ColabFold notebook [50,51] The model with the highest confidence score (pLDDT, rank_001) was selected for analysis.

Amyloidogenic potential was screened using the Waltz algorithm [52]. The resulting structural model was visualized using UCSF ChimeraX [53]. To map the predicted amyloidogenic regions onto the structure, we utilized the command interface to apply a white background, grey surface rendering, and specific red coloring (color #1:start-end red) for residues identified by Waltz, allowing for the assessment of solvent exposure.

5. Conclusions

Reanalysis of ribosomal RNA–depleted brain RNA-seq datasets identified low-biomass microbial signatures that distinguished advanced Alzheimer's disease (AD) dorsolateral prefrontal cortex (DLPFC) samples from controls, with Acinetobacter radioresistens showing the most consistent association with AD status. These observations complement increasing interest in infection- and dysbiosis-informed frameworks for AD, in which innate immune activation, blood–brain barrier integrity, chronic microbial exposures, and host genetic susceptibility may together shape neurodegenerative trajectories.

 doi:10.20944/preprints202603.0485.v1

As an exploratory analysis based on bulk post-mortem RNA-seq data not originally designed for microbiome profiling, our findings should be interpreted as hypothesis-generating and as a foundation for targeted follow-up studies. Future work using dedicated microbiome sequencing protocols, matched negative controls, spatially resolved approaches, and larger cohorts will be important to refine taxonomic resolution, address potential background signals in low-biomass samples, and clarify questions of microbial viability, localization, and temporal dynamics relative to neuropathology. Such studies will help determine the biological relevance of these signals and further evaluate their potential contribution to AD pathogenesis.

Funding: This work was partially funded by the "Ajuts A L'activitat De Recerca Del Personal Docent i Investigador De La Universitat Ramon Llull" (Ref. 2025-URL-Proj-007).

Data: Availability Statement All sequencing data analyzed in this study are publicly available from the NCBI Gene Expression Omnibus under accession GSE53697 and associated SRA records. Analysis steps were performed using the Galaxy platform and standard open-source tools as described in the Methods.

Conflicts of Interest: The authors declare no conflicts of interest.

Abbreviations

The following abbreviations are used in this manuscript:

SD	Standard Deviation
FC	Fold Change
AD	Alzheimer's disease
SEM	Standard Error of the Mean

References

1. Selkoe, D. J.; Hardy, J. 2016. The amyloid hypothesis of Alzheimer's disease at 25 years. EMBO Molecular Medicine, 8(6), 595–608.
2. van Dyck, C. H.; Swanson, C. J.; Aisen, P.; et al. 2023. Lecanemab in early Alzheimer's disease. New England Journal of Medicine, 388, 9–21.
3. Sims JR, Zimmer JA, Evans CD, et al. 2023. Investigators. Donanemab in Early Symptomatic Alzheimer Disease: The TRAILBLAZER-ALZ 2 Randomized Clinical Trial. JAMA. 330(6):512-527
4. Kunkle, B. W.; Grenier-Boley, B.; Sims, R.; Bis, J. C.; Damotte, V.; Naj, A. C.; et al. 2019. Genetic meta-analysis of diagnosed Alzheimer's disease identifies new risk loci and implicates Aβ, tau, immunity and lipid processing. Nature Genetics, 51, 414–430.
5. Piacentini R, De Chiara G, Li Puma DD, et al. 2014. HSV-1 and Alzheimer's disease: more than a hypothesis. Front Pharmacol. 5:97.
6. Readhead, B.; Haure-Mirande, J.-V.; Funk, C. C.; et al. 2018. Multiscale analysis of independent Alzheimer's cohorts finds disruption of molecular, genetic, and clinical networks by human herpesvirus. Neuron, 99(1), 64–82.e7.
7. Rizzo, R. 2020. Controversial role of herpesviruses in Alzheimer's disease. PLoS Pathogens, 16(6), e1008575.
8. Allnutt, M. A.; Johnson, K.; Bennett, D. A.; Connor, S. M.; Troncoso, J. C.; Pletnikova, O.; Albert, M. S.; De Jager, P. L.; Jacobson, S. 2020. Human herpesvirus 6 (HHV-6) detection in Alzheimer's disease cases and controls across multiple cohorts. Neuron, 105(6), 1027–1035.e2.
9. Dominy SS, Lynch C, Ermini F, Benedyk M, Marczyk A, Konradi A, Nguyen M, Haditsch U, Raha D, Griffin C, Holsinger LJ, Arastu-Kapur S, Kaba S, Lee A, Ryder MI, Potempa B, Mydel P, Hellvard A, Adamowicz K, Hasturk H, Walker GD, Reynolds EC, Faull RLM, Curtis MA, Dragunow M, Potempa J. 2019. Porphyromonas gingivalis in Alzheimer's disease brains: Evidence for disease causation and treatment with small-molecule inhibitors. Science Advances, 5(1), eaau3333.
10. Villar A, Paladini S, Cossatis J. 2024. Periodontal disease and Alzheimer's: Insights from a systematic literature network analysis. Journal of Prevention of Alzheimer's Disease. 11(4):1148-1165

 doi:10.20944/preprints202603.0485.v1

11. Sarmiento-Ordóñez JM, Brito-Samaniego DR, Vásquez-Palacios AC, Pacheco-Quito EM. 2025. Association between Porphyromonas gingivalis and Alzheimer's disease in older adults: A comprehensive review. Infection and Drug Resistance. 18:2119-2136.
12. Soscia SJ, Kirby JE, Washicosky KJ, Tucker SM, Ingelsson M, Hyman B, Burton MA, Goldstein LE, Duong S, Tanzi RE, Moir RD. 2010. The Alzheimer's disease-associated amyloid β-protein is an antimicrobial peptide. PLoS ONE, 5(3), e9505.
13. Moir, R. D.; Lathe, R.; Tanzi, R. E. 2018. The antimicrobial protection hypothesis of Alzheimer's disease. Alzheimer's & Dementia, 14(12), 1602–1614.
14. Eimer WA, Vijaya Kumar DK, Navalpur Shanmugam NK, Rodriguez AS, Mitchell T, Washicosky KJ, György B, Breakefield XO, Tanzi RE, Moir RD. 2018. Alzheimer's disease-associated β-amyloid is rapidly seeded by Herpesviridae to protect against brain infection. Neuron, 99(1), 56–63.e3.
15. Friedland, R. P.; Chapman, M. R. 2017. The role of microbial amyloid in neurodegeneration. PLoS Pathogens, 13(12), e1006654.
16. Venegas C, Kumar S, Franklin BS, Dierkes T, Brinkschulte R, Tejera D, Vieira-Saecker A, Schwartz S, Santarelli F, Kummer MP, Griep A, Gelpi E, Beilharz M, Riedel D, Golenbock DT, Geyer M, Walter J, Latz E, Heneka MT. 2017. Microglia-derived ASC specks cross-seed amyloid-β in Alzheimer's disease. Nature, 552 (7685), 355–361.
17. Taquet M, Dercon Q, Todd JA, Harrison PJ. 2024. The recombinant shingles vaccine is associated with lower risk of dementia. Nature Medicine, 30(10):2777-2781.
18. Eyting M, Xie M, Michalik F, Heß S, Chung S, Geldsetzer P. 2025. A natural experiment on the effect of herpes zoster vaccination on dementia. Nature, 641(8062):438-446.
19. Salter SJ, Cox MJ, Turek EM, Calus ST, Cookson WO, Moffatt MF, Turner P, Parkhill J, Loman NJ, Walker AW. 2014. Reagent and laboratory contamination can critically impact sequence-based microbiome analyses. BMC Biology, 12, 87.
20. Eisenhofer, R.; Minich, J. J.; Marotz, C.; Cooper, A.; Knight, R.; Weyrich, L. S. 2019. Contamination in low microbial biomass microbiome studies: Issues and recommendations. Trends in Microbiology, 27(2), 105–117.
21. Fierer N, Leung PM, Lappan R, Eisenhofer R, Ricci F, Holland SI, Dragone N, Blackall LL, Dong X, Dorador C, Ferrari BC, Goordial J, Holmes SP, Inagaki F, Korem T, Li SS, Makhalanyane TP, Metcalf JL, Nagarajan N, Orsi WD, Shanahan ER, Walker AW, Weyrich LS, Gilbert JA, Willis AD, Callahan BJ, Shade A, Parkhill J, Banfield JF, Greening C. 2025. Guidelines for preventing and reporting contamination in low-biomass microbiome studies. Nat Microbiol. 10(7):1570-1580.
22. Wang M, Beckmann ND, Roussos P, Wang E, Zhou X, Wang Q, Ming C, Neff R, Ma W, Fullard JF, Hauberg ME, Bendl J, Peters MA, Logsdon B, Wang P, Mahajan M, Mangravite LM, Dammer EB, Duong DM, Lah JJ, Seyfried NT, Levey AI, Buxbaum JD, Ehrlich M, Gandy S, Katsel P, Haroutunian V, Schadt E, Zhang B. 2018. The Mount Sinai cohort of large-scale genomic, transcriptomic and proteomic data in Alzheimer's disease. Scientific Data, 5, 180185.
23. Amabebe, E.; Anumba, D. O. C. 2018. The vaginal microenvironment: The physiologic role of Lactobacilli. Frontiers in Medicine, 5, 181.
24. Zheng, N.; Guo, R.; Wang, J.; Zhou, W.; Ling, Z. 2021. Contribution of Lactobacillus iners to vaginal health and diseases: A systematic review. Frontiers in Cellular and Infection Microbiology, 11, 792787.
25. Vaneechoutte, M. 2017. Lactobacillus iners, the unusual suspect. Research in Microbiology, 168(9–10), 826–836.
26. 26. Suzuki A, Stern SA, Bozdagi O, Huntley GW, Walker RH, Magistretti PJ, Alberini CM. 2011. Astrocyte–neuron lactate transport is required for long-term memory formation. Cell, 144(5), 810–823.
27. 27. Yang J, Ruchti E, Petit JM, Jourdain P, Grenningloh G, Allaman I, Magistretti PJ. 2014. Lactate promotes plasticity gene expression by potentiating NMDA signaling in neurons. Proceedings of the National Academy of Sciences USA, 111(33), 12228–12233.
28. 28. Barka, E. A.; Vatsa, P.; Sanchez, L.; Gaveau-Vaillant, N.; Jacquard, C.; Klenk, H.-P.; Clément, C.; Ouhdouch, Y.; van Wezel, G. P. 2015. Taxonomy, physiology, and natural products of Actinobacteria. Microbiology and Molecular Biology Reviews, 80(1), 1–43.

 doi:10.20944/preprints202603.0485.v1

29. 29. Ma, Y.; Wang, J.; Liu, Y.; Wang, X.; Zhang, B.; Zhang, W.; Chen, T.; Liu, G.; Xue, L.; Cui, X. 2023. Nocardioides: “Specialists” for hard-to-degrade pollutants in the environment. Molecules, 28(21), 7433.
30. 30. Hritcu, L.; Stefan, M.; Brandsch, R.; Mihasan, M. 2013. 6-hydroxy-L-nicotine from Arthrobacter nicotinovorans sustain spatial memory formation by decreasing brain oxidative stress in rats. Journal of Physiology and Biochemistry, 69(1), 25–34.
31. 31. Hritcu L, Stefan M, Brandsch R, Mihasan M. 2015. Enhanced behavioral response by decreasing brain oxidative stress to 6-hydroxy-L-nicotine in Alzheimer’s disease rat model. Neuroscience Letters, 591, 41–47.
32. 32. Boiangiu RS, Mihasan M, Gorgan DL, Stache BA, Petre BA, Hritcu L. 2020. Cotinine and 6-hydroxy-L-nicotine reverse memory deficits and reduce oxidative stress in Aβ25–35-induced rat model of Alzheimer’s disease. Antioxidants, 9(8), 768.
33. 33. Montagne A, Barnes SR, Sweeney MD, Halliday MR, Sagare AP, Zhao Z, Toga AW, Jacobs RE, Liu CY, Amezcua L, Harrington MG, Chui HC, Law M, Zlokovic BV. 2015. Blood–brain barrier breakdown in the aging human hippocampus. Neuron, 85(2), 296–302.
34. 34. Nation DA, Sweeney MD, Montagne A, Sagare AP, D'Orazio LM, Pachicano M, Sepehrband F, Nelson AR, Buennagel DP, Harrington MG, Benzinger TLS, Fagan AM, Ringman JM, Schneider LS, Morris JC, Chui HC, Law M, Toga AW, Zlokovic BV. 2019. Blood–brain barrier breakdown is an early biomarker of human cognitive dysfunction. Nature Medicine, 25, 270–276.
35. 35. De Gregorio, E.; Del Franco, M.; Martinucci, M.; Roscetto, E.; Zarrilli, R.; Di Nocera, P. P. 2015. Biofilm-associated proteins: news from Acinetobacter. BMC Genomics, 16, 933.
36. 36. Noble JM, Scarmeas N, Celenti RS, Elkind MS, Wright CB, Schupf N, Papapanou PN. 2014. Serum IgG antibody levels to periodontal microbiota are associated with incident Alzheimer disease. PLoS ONE, 9(12), e114959. 50. Poole, S.; Singhrao, S. K.; Kesavalu, L.; Curtis, M. A.; Crean, S. 2013. Determining the presence of periodontopathic virulence factors in short-term postmortem Alzheimer’s disease brain tissue. Journal of Alzheimer’s Disease, 36(4), 665–677.
37. 37. Pereira AJDSPR, Tavares AT, Prates M, Ribeiro N, Fonseca LF, Marques MDR, Proença F. 2022. Brain abscess: A rare clinical case with oral etiology. Case Rep Infect Dis, 2022:5140259.
38. 38. Emery DC, Shoemark DK, Batstone TE, Waterfall CM, Coghill JA, Cerajewska TL, Davies M, West NX, Allen SJ. 2017. 16S rRNA next generation sequencing analysis shows bacteria in Alzheimer’s post-mortem brain. Frontiers in Aging Neuroscience, 9, 195.
39. 39. Alonso R, Pisa D, Fernández-Fernández AM, Carrasco L. 2018. Infection of fungi and bacteria in brain tissue from elderly persons and patients with Alzheimer’s disease. Frontiers in Aging Neuroscience, 10, 159.
40. 40. Ravaioli S, De Donno A, Bottau G, Campoccia D, Maso A, Dolzani P, Balaji P, Pegreffi F, Daglia M, Arciola CR. 2024. The Opportunistic Pathogen Staphylococcus warneri: Virulence and Antibiotic Resistance, Clinical Features, Association with Orthopedic Implants and Other Medical Devices, and a Glance at Industrial Applications. Antibiotics (Basel), 13(10), 972. or products referred to in the content.
41. Leinonen, R.; Sugawara, H.; Shumway, M. 2011. The Sequence Read Archive. Nucleic Acids Research, 39(Database issue), D19–D21.
42. Afgan E, Baker D, Batut B, van den Beek M, Bouvier D, Cech M, Chilton J, Clements D, Coraor N, Grüning BA, Guerler A, Hillman-Jackson J, Hiltemann S, Jalili V, Rasche H, Soranzo N, Goecks J, Taylor J, Nekrutenko A, Blankenberg D. 2018. The Galaxy platform for accessible, reproducible and collaborative biomedical analyses: 2018 update. Nucleic Acids Research, 46(W1):W537-W544.
43. Andrews, S. 2010. FastQC: A quality control tool for high throughput sequence data. Babraham Bioinformatics.
44. Bolger, A. M.; Lohse, M.; Usadel, B. 2014. Trimmomatic: A flexible trimmer for Illumina sequence data. Bioinformatics, 30(15), 2114–2120.
45. Wood, D. E.; Lu, J.; Langmead, B. 2019. Improved metagenomic analysis with Kraken 2. Genome Biology, 20(1), 257.
46. Lu, J.; Breitwieser, F. P.; Thielen, P.; Salzberg, S. L. 2017. Bracken: Estimating species abundance in metagenomics data. PeerJ Computer Science, 3, e104.

 doi:10.20944/preprints202603.0485.v1

47. Ondov, B. D.; Bergman, N. H.; Phillippy, A. M. 2011. Interactive metagenomic visualization in a Web browser. BMC Bioinformatics, 12, 385.
48. Chong, J.; Liu, P.; Zhou, G.; Xia, J. 2020. Using MicrobiomeAnalyst for comprehensive statistical, functional, and meta-analysis of microbiome data. Nature Protocols, 15, 799–821.
49. Robinson, M. D.; McCarthy, D. J.; Smyth, G. K. 2010. edgeR: a Bioconductor package for differential expression analysis of digital gene expression data. Bioinformatics, 26(1), 139–140.
50. Jumper J, Evans R, Pritzel A, Green T, Figurnov M, Ronneberger O, Tunyasuvunakool K, Bates R, Žídek A, Potapenko A, Bridgland A, Meyer C, Kohl SAA, Ballard AJ, Cowie A, Romera-Paredes B, Nikolov S, Jain R, Adler J, Back T, Petersen S, Reiman D, Clancy E, Zielinski M, Steinegger M, Pacholska M, Berghammer T, Bodenstein S, Silver D, Vinyals O, Senior AW, Kavukcuoglu K, Kohli P, Hassabis D. 2021. Highly accurate protein structure prediction with AlphaFold. Nature, 596(7873), 583–589.
51. Mirdita, M.; Schütze, K.; Moriwaki, Y.; Heo, L.; Ovchinnikov, S.; Steinegger, M. 2022. ColabFold: making protein folding accessible to all. Nature Methods, 19(6), 679–682.
52. Maurer-Stroh S, Debulpaep M, Kuemmerer N, Lopez de la Paz M, Martins IC, Reumers J, Morris KL, Copland A, Serpell L, Serrano L, Schymkowitz JW, Rousseau F. 2010. Exploring the sequence determinants of amyloid structure using position-specific scoring matrices. Nature Methods, 7(3), 237–242.
53. Pettersen EF, Goddard TD, Huang CC, Meng EC, Couch GS, Croll TI, Morris JH, Ferrin TE. 2021. UCSF ChimeraX: Structure visualization for researchers, educators, and developers. Protein Science, 30(1), 70–82.